

Methane efflux from boreal wetlands: Theory and testing of the ecosystem model Ecosys with chamber and tower flux measurements

R. F. Grant

Department of Renewable Resources, University of Alberta, Edmonton, Alberta, Canada

N. T. Roulet

Department of Geography and Centre for Climate and Global Change Research, McGill University, Montreal, Quebec, Canada

Received 24 September 2001; accepted 10 January 2002; published 9 October 2002.

[1] A robust model of CH₄ emission from terrestrial ecosystems should be capable of simulating the temporal and spatial variability that characterizes field measurements. Such a model should couple a biologically based treatment of microbial CH₄ transformations with a physically based treatment of heat, solute, and gas transfer vertically and laterally through soils. These processes are coupled in the ecosystem model Ecosys, which was tested against CH₄ effluxes measured with surface chambers and a flux tower at a beaver pond in the BOREAS Northern Study Area. Spatial and temporal variation of CH₄ effluxes in the model encompassed that measured by surface chambers and the flux tower. Both modeled and measured CH₄ effluxes rose from <0.05 μmol m⁻² s⁻¹ and <0.01 g C m⁻² d⁻¹ at sites above the pond to >1.0 μmol m⁻² s⁻¹ and >0.5 g C m⁻² d⁻¹ at the pond margin. Larger effluxes occurred in the model when warming pond sediments generated episodic bubbling events. Annual CH₄ effluxes in the model rose from <1 g C m⁻² at sites above the pond to 76 g C m⁻² at the pond margin. Annual totals included several brief but rapid efflux events during thawing and warming of soil and pond sediments that are frequently missed by surface measurements. Annual CH₄ effluxes predicted after 100 years under an IS92a-driven climate change scenario rose by ~20% from the pond, but changed little from the surrounding landscape, indicating topographic variation in response of CH₄ effluxes to climate change. *INDEX TERMS:* 0315

Atmospheric Composition and Structure: Biosphere/atmosphere interactions; 1890 Hydrology: Wetlands; *KEYWORDS:* Ecosys, methane emissions, wetlands, modeling

Citation: Grant, R. F., and N. T. Roulet, Methane efflux from boreal wetlands: Theory and testing of the ecosystem model Ecosys with chamber and tower flux measurements, *Global Biogeochem. Cycles*, 16(4), 1054, doi:10.1029/2001GB001702, 2002.

1. Introduction

[2] The emission to the atmosphere of CH₄ from natural wetlands has been estimated to be about 115 Tg yr⁻¹, which is 20% of that from all terrestrial sources [Cicerone and Oremland, 1988; Fung et al., 1991; Melillo et al., 1996]. Boreal wetlands may emit about 20 Tg CH₄ yr⁻¹ [Bartlett and Harriss, 1993], of which as much as 32% may be from beaver ponds in some regions [Roulet et al., 1992]. However, the accuracy of these estimates is uncertain because CH₄ emission arises from complex interactions among fermentative, methanogenic, and methanotrophic processes that vary nonlinearly with soil O₂, temperature, and C content, all of which vary temporally and spatially. Emis-

sion is further affected by different transfer processes, including bubbling, convection, diffusion, and ventilation through plant roots. Consequently, CH₄ emissions vary with water table depth [Martikainen et al., 1993; Fechner and Hemmond, 1992], temperature [Dunfield et al., 1993; Frolking and Crill, 1994], phytomass [Whiting and Chanton, 1992], and net primary productivity [Aselmann and Crutzen, 1990].

[3] The complexity and the spatial and temporal variability of the processes controlling CH₄ emissions have limited the accuracy with which these emissions can be measured and aggregated [Moore and Knowles, 1990; Moosavi and Crill, 1997]. Consequently, mathematical modeling has been used to estimate CH₄ fluxes over soils. Surface CH₄ fluxes measured over wetlands have been regressed on soil temperature, soil water content, depth to water table, and precipitation [e.g., Dalva et al., 2001; Friborg et al., 2000; Frolking and Crill, 1994]. These

regressions have then been used with soil climate models to simulate seasonal changes in daily CH₄ fluxes at the same sites as those of parameterization, but cannot be used elsewhere. A problem with these regressions is that much of the variation in surface CH₄ fluxes cannot be explained by soil conditions [Frolking and Crill, 1994]. In a more mechanistic approach, daily CH₄ fluxes have been simulated from calculated rates of organic matter and litterfall decomposition, modified by soil conditions such as redox potential, pH, temperature, nutrient status, and water table depth [e.g., Cao *et al.*, 1995; Potter *et al.*, 2001]. The importance of organic C inputs to CH₄ emissions was recognized in these models, but processes for microbiological transformations and physical transport of CH₄ that control these emissions were not explicitly represented. Consequently, these models may not simulate the large temporal variation commonly observed in surface CH₄ fluxes.

[4] There have been some recent efforts to model these processes more explicitly. Walter and Heimann [2000] spatially resolved the microbiological transformations of CH₄ into methanogenesis and methanotrophy and resolved the physical transport of CH₄ into soil and plant diffusion and ebullition. This model was able to simulate CH₄ emissions under diverse site conditions, but required site-specific evaluation of critical parameters for both microbiological and physical processes. Such evaluation indicated a need for more explicit modeling of plant litterfall, root distribution, soil gases, and microbial kinetics. Segers and Leffelaar [2001a] modeled these processes more explicitly by including substrate-driven methanogenesis and methanotrophy as affected by O₂ and other soil gases, other electron acceptors, and root geometry. This model was able to simulate the general range of CH₄ emissions at wetland sites in the Netherlands [Segers and Leffelaar, 2001b]. However, it did not simulate the large spatial and seasonal variation in these emissions, possibly because rates and vertical distributions of plant C inputs were prescribed rather than dynamically simulated.

[5] A more biologically based approach than that used to model CH₄ emission in soils has been used to model that in bioreactors [e.g., Mosey, 1983; Shea *et al.*, 1968]. This approach is based on the stoichiometries, kinetics, and yields of the microbial populations involved in fermentation, methanogenesis, and methanotrophy. If adapted to soils, this approach could lead to a robust model of CH₄ emission that would be applicable under diverse soils and climates because model parameters could be derived from basic studies of CH₄ biochemistry and independently from site-specific measurements of CH₄ fluxes. The adaptation of this approach to soils would require that substrates for fermentation be generated from dynamic models of plant C fixation and litterfall, and that substrates and products of fermentation, methanogenesis, and methanotrophy undergo aqueous and gaseous transport through spatially inhomogeneous soils. The implementation of a biologically based simulation of CH₄ emission from soil was undertaken as part of the Ecosys modeling project [Grant, 2001] to improve the confidence with which soil CH₄ fluxes could be estimated under diverse environmental conditions. The simulation was based on the assumptions that

(1) CH₄ emission can be represented from the interrelated activities of four microbial communities defined by functional type: anaerobic fermenters and H₂-producing acetogens, acetotrophic methanogens, hydrogenotrophic methanogens, and autotrophic methanotrophs and (2) the transfer of substrates and products by which the activities of these communities is determined can be represented by convective and diffusive processes in aqueous and gaseous phases of soils and plants. The validity of these assumptions has been tested against CH₄ emissions and uptake reported from soil columns incubated with different organic amendments at different temperatures and water contents [Grant, 1998, 1999]. The assumptions are now examined to see if they allow simulation of the temporal and spatial variability of CH₄ emissions from a boreal wetland as measured with surface chambers and flux towers as part of the Boreal Ecosystem Atmosphere Study (BOREAS).

[6] If supported, these assumptions could provide a robust predictive capability for CH₄ emissions from diverse terrestrial ecosystems. A key application of this predictive capability is the estimation of how CH₄ emissions from boreal wetlands might change under hypothesized changes in climate caused by rising concentrations of CO₂ in the atmosphere (C_a). The model is therefore used to estimate changes in annual CH₄ emissions after 100 years under the climate change trajectory believed to be caused by the IS92a CO₂ emissions scenario.

2. Model Development

2.1. Summary of Soil Biology

[7] The hypotheses for CH₄ transformations are part of a larger model of soil C, N, and P transformations [Grant *et al.*, 1993a, 1993b] driven by energy yields from oxidation-reduction reactions. This model is based on six organic states among which C, N, and P may move: solid organic matter (S), soluble organic matter (P), sorbed organic matter (B), acetate (A), microbial communities (M), and microbial residues (Z). Each state is resolved into between two and four hierarchical levels of biological organization, listed below from higher to lower, for which the descriptors *i*, *n*, *k*, and *m* are used:

- i* organic matter-microbe complex;
- n* functional type within each complex (microbial populations only);
- j* structural or kinetic components within each complex or functional type;
- k* elemental fraction within each structural or kinetic component

Thus the solid organic matter (S) in each layer of a heterogeneous soil profile is represented in each of four independent organic matter-microbe complexes *S_i* where *i* = animal manure, plant residue, active soil organic matter, or passive soil organic matter. Each *S_i* is further resolved into kinetic components *S_{i,j}* each of which is assumed to be a homogeneous substrate of differing resistance to microbial decomposition. For example, *S_y* (where *y* = plant residue) is resolved into components of protein, carbohydrate, cellulose, and lignin. Each component consists of elemental fractions *S_{i,j,k}* where *k* = carbon, nitrogen or phosphorus.

[8] Each S_i is associated with a heterotrophic microbial community M_i resolved into functional types $M_{i,n}$ where n = obligately aerobic bacteria [Grant *et al.*, 1993a, 1993b], facultatively anaerobic denitrifiers [Grant *et al.*, 1993c, 1993d; Grant and Pattey, 1999], fungi, anaerobic fermenters plus H_2 -producing acetogens, acetotrophic methanogens [Grant, 1998], and non-symbiotic diazotrophs. There is also an autotrophic microbial community that includes NH_4^+ and NO_2^- oxidizers [Grant, 1994, 1995], hydrogenotrophic methanogens [Grant, 1998] and methanotrophs [Grant, 1999]. Each $M_{i,n}$ has structural components $M_{i,n,j}$ where j can be labile, resistant, or storage which are used to calculate kinetic components j which can be active or quiescent. Each $M_{i,n,j}$ consists of fractions $M_{i,n,j,k}$ where k can be carbon, nitrogen, or phosphorus. A general flow diagram for the transformation of material in the soil ecosystem is given by Grant *et al.* [1993a, Figures 1 and 2], and a hierarchical table of state variables is given by Grant [1999, Table 1]. A more detailed description of soil CH_4 transformations is given below with reference to equations listed in Appendix A.

2.2. Summary of Plant Biology

[9] Plant residue $S_{y,j,k}$ receives litterfall from a biologically based model of multispecific plant growth, senescence, and exudation driven by autotrophic CO_2 fixation and respiration. Autotrophic CO_2 fixation is calculated from radiation, air temperature and C_a , and by plant nutrient (N and P) and water status [Grant, 2001; Grant *et al.*, 2001a, 2001b]. Autotrophic respiration is the sum of growth and maintenance components. Shoot and root litterfall occurs when respiration exceeds CO_2 fixation enough to deplete shoot and root C reserves. Root exudation is driven by root C reserve concentration. Shoot litterfall is added to a surface residue layer maintained as a separate entity on the soil surface, and root litterfall plus exudation is added to soil layers according to a root-mycorrhizal growth model driven by shoot-root-mycorrhizal exchange of C and nutrients.

2.3. Anaerobic Fermenters and H_2 Producing Acetogens

[10] The states $S_{i,j,k}$, $B_{i,k}$ and $Z_{i,j,k}$ in Ecosys are substrates for hydrolysis by all active ($j = a$) heterotrophic biomass communities $M_{i,n,a}$ [Grant *et al.*, 1993a, equations (1)–(7)], which include fermenters plus acetogens. Hydrolysis products are transferred to soluble organic matter $P_{i,k}$ which is the substrate for respiration and uptake by microbial biomass $M_{i,n,j}$ as described for aerobic heterotrophs by Grant *et al.* [1993a, equation (11)]. Respiration $R_{i,f}$ of $P_{i,c}$ by fermenters plus acetogens ($n = f$) is a Michaelis-Menten function of $[P_{i,c}]$ inhibited by O_2 (equation (1)). Respiration products are partitioned among $A_{i,c}$, CO_2 , and H_2 according to Brock and Madigan [1991] (equation (2)). $R_{i,f}$ beyond that used for maintenance respiration drives the uptake of additional $P_{i,c}$ (equations (3a) and (3b)) for microbial growth according to the growth yield Y_f of fermentation (equation (4)). The growth yield from fermentation is calculated by dividing the free energy change of fermentation, adjusted for H_2 product concentration (equation (5)), by the energy required to transform soluble organic C into microbial C (equation (4)). Change in $M_{i,f,j}$ is thus the

difference between uptake and respiration of $P_{i,c}$, less decomposition (equations (6a) and (6b)). This change determines $M_{i,f,a}$ used in the following calculation of $R_{i,f}$ (equation (1)). Ratios of $M_{i,f,j,c}$ to $M_{i,f,j,n}$ determine mineralization-immobilization of N [Grant *et al.*, 1993a, equation (23)]. Decomposition products $D_{i,f,j,k}$ are partitioned to microbial residues $Z_{i,j,k}$ and soil organic matter $S_{i,j,k}$ (where i = passive soil organic matter) [Grant *et al.*, 1993a, equations (26)–(28)] which undergo further hydrolysis.

2.4. Acetotrophic Methanogens

[11] The fermenter product $A_{i,c}$ (equation (2)) is the substrate for respiration $R_{i,m}$ by acetotrophic methanogens ($n = m$) (equation (7)). Respiration products are partitioned between CH_4 and CO_2 according to Brock and Madigan [1991] (equation (8)). $R_{i,m}$ beyond that used for maintenance respiration drives the uptake of additional $A_{i,c}$ (equations (9a) and (9b)) for microbial growth according to the growth yield Y_m of acetotrophic methanogenesis (equation (10)). This growth yield is calculated by dividing the free energy change of acetotrophic methanogenesis [Brock and Madigan, 1991] by the energy required to transform acetate into microbial C. Acetogenic methanogens in the model use acetate as their sole carbon and energy source [Smith and Mah, 1980]. Change in $M_{i,m,j}$ is thus the difference between uptake and respiration of $A_{i,c}$, less decomposition (equations (11a) and (11b)). This change determines $M_{i,m,a}$ used in the following calculation of $R_{i,m}$ (equation (7)). Mineralization and decomposition processes are the same as those for other microbial populations.

2.5. Hydrogenotrophic Methanogens

[12] The fermenter products CO_2 and H_2 (equation (2)) are the substrates for CO_2 reduction by hydrogenotrophic methanogens ($n = h$) which are assumed to be autotrophic (equation (12)). Respiration products are partitioned between CH_4 and H_2O according to Brock and Madigan [1991] (equation (13)). R_h beyond that used for maintenance respiration drives the uptake of additional CO_2 (equations (14a) and (14b)) for microbial growth according to the growth yield Y_h of hydrogenotrophic methanogenesis [Brock and Madigan, 1991] (equation (15)). This growth yield is calculated by dividing the free energy change of hydrogenotrophic methanogenesis, adjusted for H_2 substrate concentration (equation (16)), by the energy required to transform CO_2 into microbial C. Change in $M_{h,j}$ is thus the difference between uptake and respiration of CO_2 , less decomposition (equations (17a) and (17b)). This change determines $M_{h,3a}$ used in the following calculation of R_h (equation (12)). Mineralization and decomposition processes are the same as those for other microbial populations.

2.6. Autotrophic Methanotrophs

[13] Methane generated by acetotrophic and hydrogenotrophic methanogens is the substrate for CH_4 oxidation by autotrophic methanotrophs ($n = t$) (equation (18)). The stoichiometry and energetics of the methanotrophic reactions (equations (22)–(24)) are based on those of CH_4 to CO_2 given by Brock and Madigan [1991]. The oxidation of CH_4 to CO_2 is coupled through an energy yield with the

Table 1. Values of Parameters Provided to the Model

Parameter	Equation	Value	Source
D'_{CH_4}	[32, 39]	$7.80 \times 10^{-2} \text{ m}^2 \text{ h}^{-1}$	
D_{CH_4}	[30, 37]	$7.08 \times 10^{-6} \text{ m}^2 \text{ h}^{-1}$	<i>Wilhelm et al.</i> [1977]
E_C	[15]	75 kJ g $\text{CO}_2\text{-C}^{-1}$	
E_G	[20]	23.5 kJ g $\text{CH}_4\text{-C}^{-1}$	<i>Anthony</i> [1982]
E_M	[4, 10, 26]	25 kJ g org. C^{-1}	
$\Delta G'_c$	[26]	-37.5 kJ g $\text{CH}_2\text{O-C}^{-1}$	<i>Brock and Madigan</i> [1991]
$\Delta G'_f$	[5]	-4.43 kJ g glucose- C^{-1}	<i>Brock and Madigan</i> [1991]; <i>Schink</i> [1997]
$\Delta G'_h$	[16]	-0.27 kJ g $\text{CO}_2\text{-C}^{-1}$	<i>Brock and Madigan</i> [1991]
$\Delta G'_m$	[10]	-1.03 kJ g acetate- C^{-1}	<i>Brock and Madigan</i> [1991], <i>Schink</i> [1997]
$\Delta G'_t$	[20]	-9.45 kJ g $\text{CH}_4\text{-C}^{-1}$	<i>Brock and Madigan</i> [1991]
$[\text{H}_2]$	[5, 16]	150 $\mu\text{g H m}^{-3}$	<i>Brock and Madigan</i> [1991]
K_c	[12]	0.12 g C m^{-3}	
K_f	[1]	36 g C m^{-3}	<i>McGill et al.</i> [1981]
K_h	[12]	0.01 g H m^{-3}	<i>Mosey</i> [1983], <i>Robinson and Tiedje</i> [1982]
K_m	[7]	12 g C m^{-3}	<i>Smith and Mah</i> [1978], <i>Zehnder et al.</i> [1980]
K_r	[18]	3×10^{-3} g C m^{-3}	<i>Conrad</i> [1984]
M_{CH_4}	[40, 41]	12 g mol^{-1}	
p	[40]	101.4 kPa	
R	[5, 16, 40]	8.3143×10^{-3} kJ $\text{mol}^{-1} \text{ K}^{-1}$	
R'_f	[1]	0.40 g C g microbial C h^{-1}	<i>Lawrence</i> [1971], <i>Wofford et al.</i> [1986]
R'_h	[12]	0.12 g C g microbial C h^{-1}	<i>Shea et al.</i> [1968], <i>Zehnder and Wuhrmann</i> [1977]
R'_m	[7]	0.20 g C g microbial C h^{-1}	<i>Smith and Mah</i> [1980]
r_f	[36]	1.0×10^{-4} m	
S_{CH_4}	[28, 33, 35, 40, 41]	0.03156	<i>Wilhelm et al.</i> [1977]
τ_s	[30, 37]	0.75	
u_{gr}	[39]	1.33	<i>Luxmoore et al.</i> [1970]
u_{gs}	[32]	3.33	<i>Millington</i> [1959]
u_s	[30, 37]	2	
X'_t	[18]	0.5 g C g mic. C h^{-1}	<i>Conrad</i> [1984]

oxidation of CH_4 to organic C used in microbial respiration (equation (19)). The energy yield from CH_4 oxidation is calculated by dividing the free energy change of CH_4 oxidation by the energy required to transform CH_4 into organic C (equation (20)). Oxygen requirements to sustain CH_4 oxidation rates are then calculated from the stoichiometries of CH_4 oxidation (equations (22) and (23)) and aerobic microbial respiration (equation (24)). The O_2 concentrations at methanotrophic microsites are then found at which active O_2 uptake driven by requirements for CH_4 oxidation equals spherical O_2 diffusion to the microsites from the soil solution. These microsites are considered to be uniformly distributed on soil surfaces and are separated from the soil atmosphere (if present) by a water film of uniform thickness that depends upon soil water potential. The O_2 uptake by each aerobic microbial population in the model competes with that by all other aerobic microbial populations [e.g., *Grant*, 1995; *Grant and Rochette*, 1994] and is constrained by O_2 transfer rates through the gaseous and aqueous phases of the soil profile. The ratio of O_2 uptake to O_2 requirement f_{O_2} is then used to constrain CH_4 oxidation rates (equations (21a) and (21b)) so that CH_4 oxidation is stoichiometrically coupled to O_2 uptake. Growth respiration by methanotrophs is calculated as the difference between total respiration R_t from equation (21b) and maintenance respiration R_{m_t} from *Grant et al.* [1993a, equations (18) and (19)]. Growth respiration drives the uptake and transformation of additional CH_4 into microbial biomass $M_{t,c}$ (equations (25a) and (25b)) according to the growth yield. This yield is calculated by dividing the free energy change of CH_4 oxidation [*Brock and Madigan*, 1991] (equation (18)) by the energy required to construct

new microbial biomass from CH_4 (equation (26)). Net growth of the methanotrophic population $M_{t,j,c}$ is calculated as the uptake of $\text{CH}_4\text{-C}$ minus respiration and decomposition of assimilated C (equations (27a) and (27b)). This change determines $M_{t,a}$ used in the following calculation of X'_t (equation (18)). Mineralization and decomposition processes are the same as those for other microbial populations.

[14] This submodel of autotrophic methanotrophy has been used to simulate methanotrophic growth yields, specific growth rates, CH_4 concentration profiles, and the sensitivity of CH_4 uptake to temperature and water content in soil columns [*Grant*, 1999]. The combined submodels of anaerobic fermentation, acetotrophic methanogenesis, hydrogenotrophic methanogenesis, and autotrophic methanotrophy have been used to simulate methanogenic growth yields, specific growth rates, and the time course of CH_4 emissions from differently amended soil columns at different temperatures [*Grant*, 1998]. All input parameter values used in equations (1)–(27) (Table 1) were derived from the microbiological literature and remain unchanged from those used by *Grant* [1998, 1999].

2.7. Transport of Reactants and Products

2.7.1. Soil

[15] Methane produced by acetotrophic and hydrogenotrophic methanogens (equations (1)–(17)), and that consumed by methanotrophs (equations (18)–(27)), undergoes convective-dispersive transport through, and volatilization-dissolution transfer between, aqueous and gaseous phases of the soil and root. Transfer between gaseous and aqueous phases in each soil layer is driven by concentration differ-

ences between gaseous and aqueous phases calculated for each aqueous gas γ (CH_4 , O_2 , CO_2 , N_2 , N_2O , NH_3 , and H_2 in Ecosys) (equation (28)) from its temperature-dependent solubility [Wilhelm *et al.*, 1977]. Vertical transport between adjacent layers in the aqueous phase of the soil is calculated for each gas γ as the sum of convective and dispersive-diffusive components (equations (29) and (30)). If both these layers lack a solid phase (as in lake or pond water), the diffusive component is based on wind-driven eddy diffusivities given by Imboden and Schwarzenbach [1985]. If only the upper layer lacks a solid phase (as at the water-sediment interface), the diffusive component is based on wind-driven dispersion coefficients given by Billen [1982]. Vertical transport between adjacent layers in the gaseous phase of the soil is calculated for each gas γ as the sum of convective and diffusive components (equations (31) and (32)). The gaseous and aqueous concentration gradients by which transport is driven are generated from the production and consumption of each gas γ by roots, mycorrhizae, and microbial communities. Transport is also controlled by water-, ice-, and air-filled porosities calculated from soil heat and water fluxes driven by surface energy balances and controlled by subsurface hydrologic and thermal properties [Grant *et al.*, 1995].

[16] Vertical transport between the atmosphere and the surface layer in the aqueous phase of the soil is calculated for each gas γ such that its gaseous transport between the atmosphere and the air-surface interface is equal to its aqueous transport between the air-surface interface and the midpoint of the uppermost soil layer which is typically 0.005 m in depth (equation (33)). Vertical transport between the atmosphere and the surface layer in the gaseous phase of the soil is calculated for each gas γ such that its gaseous transport between the atmosphere and the air-surface interface is equal to its gaseous transport between the air-surface interface and the midpoint of the uppermost soil layer (equation (34)). Atmospheric transfers are governed by a wind speed-driven aerodynamic boundary layer conductance g_a , the calculation of which is described by Grant *et al.* [1995, 2001a].

2.7.2. Plant

[17] Transfer between gaseous and aqueous phases in the roots of each soil layer (equation (35)) [Grant, 1993] is calculated for each gas γ in the same way as that in the soil. Diffusive radial transport between the aqueous phases of the root and soil (equations (36) and (37)), and diffusive vertical transport between the atmosphere and the gaseous phase of the roots (equations (38) and (39)) are also calculated for each gas γ in each rooted soil layer. Aqueous and gaseous diffusivities along the soil-root-atmosphere pathway are calculated from the lengths and from the surface and cross-sectional areas of parallel secondary roots in series with parallel primary roots given by the root growth model in Ecosys. Gaseous diffusivities in the roots are also calculated from air-filled porosity based on a species-specific input value for fraction of root volume occupied by aerenchyma. The root system thus forms a pathway for gaseous transport that is parallel to that of the soil, with exchange between the two taking place through the aqueous phase of the roots.

2.7.3. Ebullition

[18] If the total gaseous equivalent concentration of all aqueous gases γ exceeds that at atmospheric pressure, an upward (negative) aqueous flux equivalent to the excess partial pressure of each gas (bubbling) is immediately transferred upward to the gaseous phase of the deepest soil layer in direct gaseous contact with the atmosphere, or directly to the atmosphere in the absence of gaseous contact (equations (40) and (41)). This transfer is not calculated if ice fully occupies the porous space in a soil layer between the bubble source and the atmosphere.

[19] Values for input parameters used in transport equations (28)–(41) are listed in Table 1. All biological transformations of C, N, and P in Ecosys are calculated hourly, while all physical transfers of water, heat, solutes, and gasses are calculated every 3 min and aggregated to hourly values. These transfers are also calculated in one or both horizontal directions (north-south and east-west) if a two- or three-dimensional model configuration is selected.

3. Methane Flux Measurements

3.1. Site Description

[20] Methane fluxes were measured at a beaver pond site ($55^\circ 55' \text{N}$; $98^\circ 01' \text{W}$) in the northern study area of the Boreal Ecosystem Atmosphere Study (BOREAS). The beaver pond was 5 ha in area and 0.25–2 m (mostly 0.5–1 m) in depth, including open water (25%), peat islands (10%), and sparse emergent (*Calamagrostis canadensis* and *Carex* spp.) and submergent vegetation (65%). The pond margin was a mire with emergent vegetation (also *Calamagrostis canadensis* and *Carex* spp.) that changed to organic soil with sphagnum moss (*Tomenthypnum nitens*) and vascular plants (*Carex* spp.) with rising elevation away from the pond. The bulk densities and the C and N contents of the beaver pond sediments were 0.093–0.105 Mg m^{-3} , 240–268 g C kg^{-1} , and 13–14 g N kg^{-1} , respectively, in the upper 0.4 m, and 0.292–0.508 Mg m^{-3} , 146–198 g C kg^{-1} , and 8–11 g N kg^{-1} , respectively, from 0.5 to 0.75 m [Roulet *et al.*, 1997].

3.2. Tower Flux Measurements Over the Beaver Pond

[21] CH_4 and CO_2 fluxes were measured over the beaver pond surface from June to September 1994 using a flux gradient technique from wind speeds recorded at heights of 0.25, 0.50, 1.00, and 1.50 m when the fetch was >90 m. Half-hourly averaged concentration gradients of CH_4 were calculated from measurements every 6 min using a gas chromatograph with a flame ionization detector (Shimadzu Mini II) (CH_4) at heights of 0.25 and 1.0 m. Further details are given by Roulet *et al.* [1997]. For model comparisons, these half-hourly fluxes were aggregated to daily totals for all days in which 40 or more values were available.

3.3. Chamber Flux Measurements Over the Beaver Pond

[22] Diffusive plus plant-mediated CH_4 fluxes were measured over open water (some submergent vegetation) and vegetated (emergent *Carex* plus submergent vegetation) sites with 18 L static floating chambers, the head-

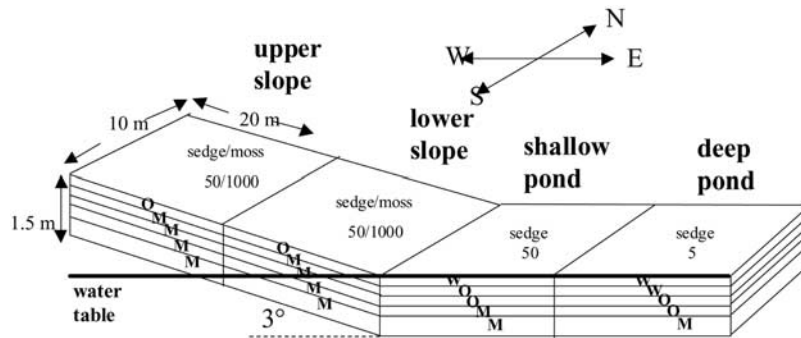


Figure 1. Landscape transect as represented in Ecosys. Soil layers: W = water, O = organic sediment (bulk density = 0.1 Mg m^{-3} , $C = 250 \text{ g kg}^{-1}$, and $N = 13 \text{ g kg}^{-1}$), and M = mineral (bulk density = $1.4 - 1.6 \text{ Mg m}^{-3}$, $C = 1 - 10 \text{ g kg}^{-1}$ and $N = 0.05 - 0.5 \text{ g kg}^{-1}$). Modeled plant species and populations (m^{-2}) are indicated for each landscape position.

spaces of which were sampled every 5 min for 20 min. Samples with nonlinear rises in CH_4 mixing ratios were rejected so that bubbling was excluded from the static chamber measurements unless it occurred at a constant rate. CH_4 mixing ratios in the headspaces were measured within 8 hours of collection using a gas chromatograph with a flame ionization detector (Shimadzu Mini II). Bubbling fluxes were measured over open water and vegetated sites with 30 cm diameter inverted funnels fitted with a cylinder and stopper through which accumulated gas was sampled every 24–48 hours. CH_4 mixing ratios in the bubbles were measured within 8 hours of collection using a gas chromatograph with a thermal conductivity detector (Shimadzu-8A). These measurements are further described by *Dove et al.* [1999].

3.4. Chamber Flux Measurements Over the Beaver Pond Margins and Surrounding Landscape

[23] CH_4 and CO_2 fluxes were measured weekly with 0.32 m diameter \times 0.36 m tall static flux chambers mounted on four plastic collars installed in mid-May 1994 at each of four positions along a 50-m transect from surrounding upland to the edge of the beaver pond. The positions were (1) an upland lichen site about 50 m from the edge of the pond and 2 m above it (water table >0.3 m below soil surface), (2) a sphagnum moss site about 20 m from the edge of the pond and about 0.5 m above it (water table periodically <0.1 m below soil surface), (3) a mire site in a backwater near the edge of the pond (water table 0.10–0.15 m above soil surface except during a 10-day drainage event at the end of June), and (4) a pond site in emergent vegetation at the edge of the pond (water table 0.10–0.15 m above soil surface except during a 10-day drainage event at the end of June). Samples of uncirculated air were drawn every 4 min. for 20 min. from each chamber between 1000 and 1600 local time. The concentrations of CH_4 in all samples were analyzed within 24 hours of collection using a flame ionization detector and a gas chromatograph (Shimadzu 14A). Soil temperatures were measured at the time of each flux measurement with thermocouples permanently installed at depths of 0.05, 0.10, and 0.20 m below the

surface. Further details are given by *Moosavi and Crill* [1997] and *BOREAS TGB-01* [1998].

4. Simulation Experiment

[24] The landscape at the BOREAS beaver pond site was represented in the model as four interconnected landscape positions along a two-dimensional transect from an upper slope position down a 3° gradient with an easterly aspect through a lower slope position to the margin of a shallow (0.2 m) pond linked to a deep (0.5 m) pond (Figure 1). Each landscape element was 20 m east-west \times 10 m north-south in area and 1.5 m deep, so that the slope was 40 m in length and 2 m in height. The elevation of the upper slope above the pond surface in the simulated landscape was the similar to that of the lichen and moss sites in the field transect. The depths of the shallow and deep pond positions below the water table in the simulated landscape were similar to those of the mire and pond sites in the field transect. The hydrology of each landscape position was simulated as that at its midpoint. Surface and subsurface downhill movement of water could occur along gravitational gradients, with associated convective and dispersive movement of heat and solutes. The basal water table (the depth below which soil saturation was maintained in the model, but above which transient saturation could occur if water infiltration exceeded evapotranspiration over time) was assumed to extend horizontally inland from the pond surface. Excess water from the simulated landscape was discharged from the pond positions as required to maintain the pond surface level.

[25] The simulated landscape was initialized with the physical and biological properties of the soil profiles at each landscape position (Figure 1). These profiles were assumed to be horizontally uniform within each landscape position with water and organic sediment layers (bulk densities and organic C and N contents of which were given in section 3.1) overlying mineral layers. The upper and lower slope positions were initialized with the biological properties of sedge (using those of grass from *Grant et al.* [2001b]) but with a greater root aerenchymous fraction

Table 2. Rates of Changes in Atmospheric Boundary Conditions Under Emissions Scenario IS92a

Boundary Condition	Change, yr ⁻¹			
	Winter	Spring	Summer	Autumn
CO ₂ concentration	+0.007	+0.007	+0.007	+0.007
Maximum daily temperature	+0.030°C	+0.025°C	+0.025°C	+0.030°C
Minimum daily temperature	+0.040°C	+0.035°C	+0.030°C	+0.035°C
Precipitation	+0.001	+0.001	+0.001	+0.001
Solar radiation	unchanged	unchanged	unchanged	unchanged
Relative humidity	unchanged	unchanged	unchanged	unchanged
Wind speed	unchanged	unchanged	unchanged	unchanged

to facilitate gas exchange) at a population of 50 m⁻² and moss (using those from *Grant et al.* [2001a]) at a population of 1000 m⁻² (Figure 1). The shallow and deep pond positions were initialized with sedge alone at populations of 50 and 5 m⁻², respectively, to simulate dense and sparse emergent vegetation reported at the pond margin and in open water. The lower boundary of each landscape position was set to prevent subsurface drainage or capillary rise, and to allow the addition or removal of water as required to maintain saturation of soil below the basal water table. The model was then run for 40 years under random yearly sequences of hourly-averaged meteorological data (air temperature, humidity and wind speed) recorded at a flux tower 30 km from the beaver pond during 1994, 1995, and 1996 [*BOREAS TF-03*, 1998], supplemented with 1-km² gridded data (shortwave radiation and precipitation) generated from surface measurements given by *Amtor et al.* [2001]. These

data were replaced by hourly-averaged air temperature, humidity, wind speed, shortwave radiation, and precipitation measured at the beaver pond flux tower while it was in operation from 22 May to 19 September 1994. Model C_a was initialized at 340 μmol mol⁻¹ and incremented daily at a rate of 0.00167 yr⁻¹ so that C_a recorded in 1994 would be reached after 40 years. Atmospheric N deposition in the model occurred as NH₄⁺ (0.5 g N m⁻³) and NO₃⁻ (0.5 g N m⁻³) dissolved in precipitation and as NH₄⁺ from adsorption of atmospheric NH₃ (0.01 μmol mol⁻¹) by leaf and soil surfaces. During the fortieth year of the model run, methane fluxes simulated as the sum of gas exchanges through plant and soil surfaces under 1994 meteorological data were compared with those measured with surface chambers and the flux tower during 1994.

[26] The model run was then extended for a further 100 years with daily increments in C_a, air temperature, and

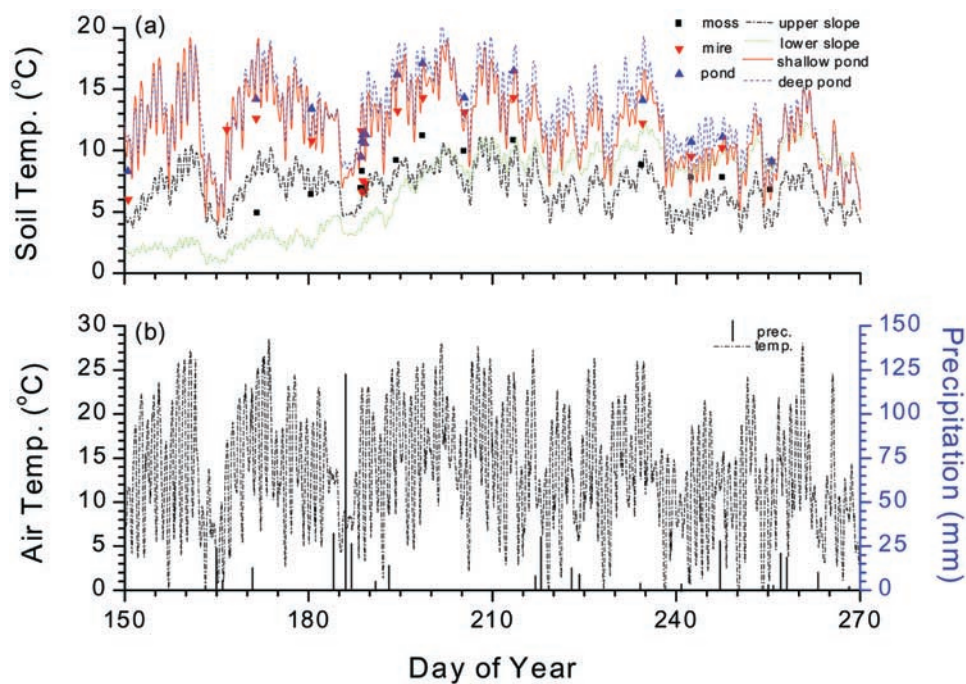


Figure 2. (a) Soil temperatures measured 0.2 m below the ground or water surface at the moss, mire, and pond sites (symbols) and simulated 0.2 m below the ground or water surface at the upper slope, lower slope, shallow pond, and deep pond positions (lines) during 1994. (b) Precipitation and air temperature measured at or near the beaver pond site during 1994. Measured temperatures are from *BOREAS TGB-01* [1998].

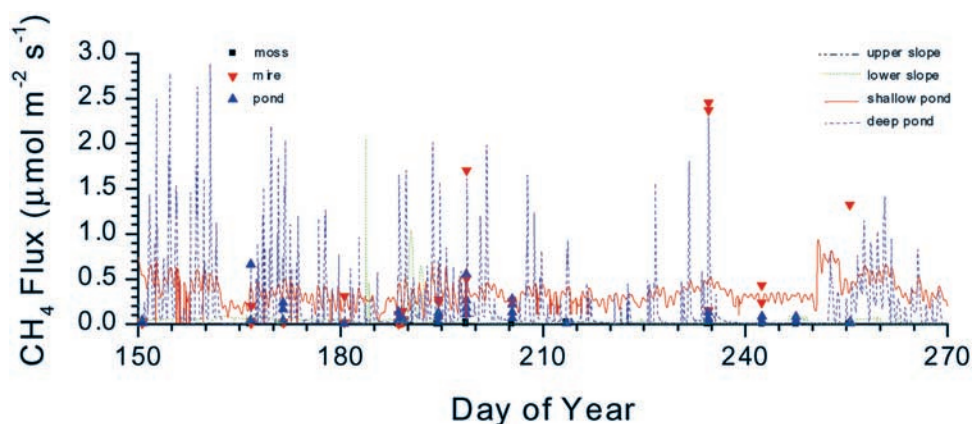


Figure 3. Hourly CH_4 effluxes measured by static surface chambers at the moss, mire, and pond sites (symbols) and simulated at the upper slope, lower slope, shallow pond, and deep pond positions (lines) during 1994. Measured effluxes are from *BOREAS TGB-01* [1998].

precipitation selected from *Kattenberg et al.* [1996] under emissions scenario IS92a (Table 2). Model output for CH_4 emissions at the end of this run was compared with that at the end of the control run.

5. Results

[27] The pond positions warmed earlier and remained 3–5°C higher than the upper slope position in the model (Figure 2a) because greater thermal mixing and the absence of a moss cover in the pond water caused more rapid heat exchange with the atmosphere. *Moosavi and Crill* [1997] measured temperatures at the mire and pond sites that were ~2° and ~4°C, respectively, higher than at the moss site of the field transect (Figure 2a). The upper slope position warmed earlier than did the lower slope position in the model (Figure 2a) because downhill water movement caused it to be better drained and hence drier. The pond and slope positions were cooled by a heavy rainfall in early July (Figure 2b).

5.1. Hourly CH_4 Effluxes

[28] Hourly CH_4 fluxes modeled at the deep pond position were temporally variable (Figure 3), with brief, large

effluxes caused by bubbling events (equations (40) and (41)) adding to steady, small effluxes caused by diffusion and plant transport (equations (28)–(39)). These bubbling events were driven by warming of the pond sediments that raised rates of fermentation and methanogenesis (f_t in equations (1), (7), and (12)), reduced total gaseous equivalent concentration at atmospheric pressure ($p/(RT)$ in equation (40)), and raised partial gaseous equivalent concentrations of aqueous gases (by reducing S'_g in equation (41)). Conversely, bubbling was suppressed by sediment cooling. The time course of modeled bubbling events during late August 1994 is shown in Figure 4. The onset of sediment warming at midday led to degassing by bubbling over several hours during the afternoons of DOY 231, 232, 234, and 235. This degassing reached peak rates of ~2 $\mu\text{mol m}^{-2} \text{s}^{-1}$, which were consistent with peak rates measured by some of the surface chambers at the mire site (Figure 3). Bubbling was suppressed by sediment cooling after DOY 235. In the absence of bubbling, CH_4 effluxes remained <0.1 $\mu\text{mol m}^{-2} \text{s}^{-1}$.

[29] Hourly CH_4 fluxes modeled at the shallow pond position were less temporally variable than those at the deep pond position (Figure 3), in part because greater root

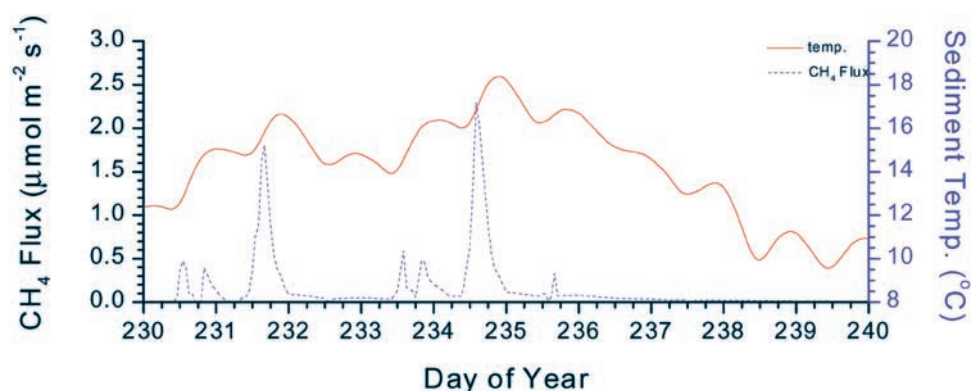


Figure 4. Hourly CH_4 effluxes and surface sediment temperatures simulated at the deep pond position from 19 to 28 August 1994 (DOY 231 to 240).

density from higher plant populations rooting in shallower sediments allowed more rapid plant transport (through larger a_{gr} in equation (35), larger L_r and smaller d_r in equation (36), and larger A_r in equation (39)) that was less sensitive to changes in temperature than was bubbling. These fluxes varied between 0.2 and 0.5 $\mu\text{mol m}^{-2} \text{s}^{-1}$ which was consistent with many of the chamber measurements at the mire and pond sites. These measurements may have been affected by a 10-day drainage event caused by a breach of the beaver dam in late June.

[30] Hourly CH_4 effluxes modeled at the lower slope position remained below 0.1 $\mu\text{mol m}^{-2} \text{s}^{-1}$ (Figure 4), except during two brief emission events in July when Effluxes briefly exceeded 1 $\mu\text{mol m}^{-2} \text{s}^{-1}$ (Figure 3). The first event occurred while the lower soil organic layer was thawing and draining during early season warming (Figure 2a), and the second occurred in mid-July while the soil was draining after heavy rainfall in early July (Figure 2b). During periods of high ice or water content in the modeled soil (e.g., during freezing or heavy rainfall), CH_4 oxidation was suppressed by low aqueous O_2 concentrations (equations (21a) and (21b)), and CH_4 diffusion was limited by low air-filled porosity (equation (32)). CH_4 therefore accumulated during these periods and was later volatilized (equation (28)) and released (equations (31) and (34)) when the soil drained or thawed. Freezing and precipitation therefore suppressed CH_4 efflux in the model, which is consistent with findings at other wetlands [e.g., *Frolking and Crill, 1994*], but caused emission events during subsequent thawing and draining.

[31] Hourly CH_4 effluxes modeled at the upper slope position remained below 0.01 $\mu\text{mol m}^{-2} \text{s}^{-1}$ during the entire season (Figure 3). These low effluxes occurred because almost all of the CH_4 generated (equations (1)–(17)) from wetter soil lower in the profile was oxidized (equations (18)–(27)) in the unsaturated zone near the soil surface [*Grant, 1999*]. The low effluxes in the model were corroborated by effluxes measured at the moss site that remained below 0.01 $\mu\text{mol m}^{-2} \text{s}^{-1}$.

[32] The increasing effluxes simulated with descent from the upper and lower slope positions to the pond positions were consistent with effluxes measured in similar wetlands elsewhere. At a subarctic fen in Quebec with a thermal regime similar to that at the beaver pond, *Moore and Knowles [1990]* measured effluxes $<0.02 \mu\text{mol m}^{-2} \text{s}^{-1}$ where the water table was 0.2 m below the peat surface (as modeled at the upper slope position), 0.01 to 0.1 $\mu\text{mol m}^{-2} \text{s}^{-1}$ where the water table was at the peat surface (as modeled at the lower slope position), and up to 0.2 $\mu\text{mol m}^{-2} \text{s}^{-1}$ when the water table was 0.4 m above the peat surface (as modeled at the pond positions). *Moore and Roulet [1995]* observed that the logarithm of CH_4 efflux from boreal and subarctic wetlands in Canada rose linearly with water table position from 0.6 m below to 0.4 m above the soil surface. On the other hand, *Moore et al. [1990]* measured lower effluxes at a flooded site in the same wetlands. *Moore and Knowles [1990]* also noted that the static chamber techniques used in these measurements may suppress turbulent exchange and thereby underestimate CH_4 effluxes from ponded sites by $\sim 20\%$.

5.2. Daily CH_4 effluxes

[33] Daily CH_4 effluxes by diffusion and bubbling measured at vegetated and open pond sites were compared with those simulated at the shallow and deep pond positions (Figure 5). Diffusive effluxes (soil plus plant) measured at vegetated pond sites varied between 0 and 0.2 $\text{g C m}^{-2} \text{d}^{-1}$ from July to September while those modeled remained $\sim 0.1 \text{g C m}^{-2} \text{d}^{-1}$ (Figure 5a). Diffusive effluxes measured at open pond sites were not modeled at the deep pond position. Larger diffusive effluxes measured during June were similar to bubble fluxes simulated during June (Figure 5b). Bubble fluxes measured at open pond sites remained $\sim 0.2 \text{g C m}^{-2} \text{d}^{-1}$ during most of the summer, similar to those simulated at the shallow pond position but frequently smaller than those simulated during bubbling events at the deep pond position (Figure 5b). Daily CH_4 effluxes measured at the flux tower were between 0 and 0.2 $\text{g C m}^{-2} \text{d}^{-1}$, similar to those modeled at the deep pond position except during bubbling events (Figure 5c). They were smaller than those modeled at the shallow pond position which was representative of only a small part of the tower fetch. Effluxes measured at the flux tower declined during late August as did those simulated, due in the model to sediment cooling (Figure 4).

5.3. Seasonal CH_4 Effluxes

[34] Seasonal totals (May–September) of CH_4 emissions modeled at the upper slope position in the modeled transect and measured at the moss site in the field transect were both $<1 \text{g C m}^{-2}$ (Table 3). Low CH_4 effluxes were modeled at this landscape position because downslope water movement prevented soil water contents from approaching saturated values. The modeled emissions rose to 5 g C m^{-2} at the lower slope position because the basal water table plus downslope water movement from the upper slope position maintained higher soil water contents. Seasonal emissions in the model rose to 46 g C m^{-2} at the shallow pond position versus 94 g C m^{-2} measured by static chambers at the mire site in the field transect, and 11 g C m^{-2} measured by static chambers plus inverted funnels at vegetated pond sites. Seasonal emissions in the model declined to 25 g C m^{-2} at the deep pond position versus 14 g C m^{-2} measured by static chambers at the pond site in the field transect, 23 g C m^{-2} measured by static chambers plus inverted funnels at open pond sites, and 8 g C m^{-2} measured at the flux tower. Larger emissions were modeled at the pond positions because most of the CH_4 was emitted through plants or bubbling, and so was not subject to oxidation. In a review of CH_4 emissions from Canadian peatlands, *Moore and Roulet [1995]* found that fens emit between 0.5 and 15 $\text{g CH}_4\text{-C m}^{-2} \text{yr}^{-1}$ (cf. 5 $\text{g CH}_4\text{-C m}^{-2} \text{yr}^{-1}$ modeled at the lower slope position) and beaver ponds emit between 5 and 95 $\text{g CH}_4\text{-C m}^{-2} \text{yr}^{-1}$ with higher emissions from shallower ($<0.5 \text{m}$) ponds (cf. 46 and 25 $\text{g CH}_4\text{-C m}^{-2} \text{yr}^{-1}$ modeled at the shallow and deep pond positions).

[35] The modeled CH_4 emissions were driven by heterotrophic oxidation-reduction of C products from primary

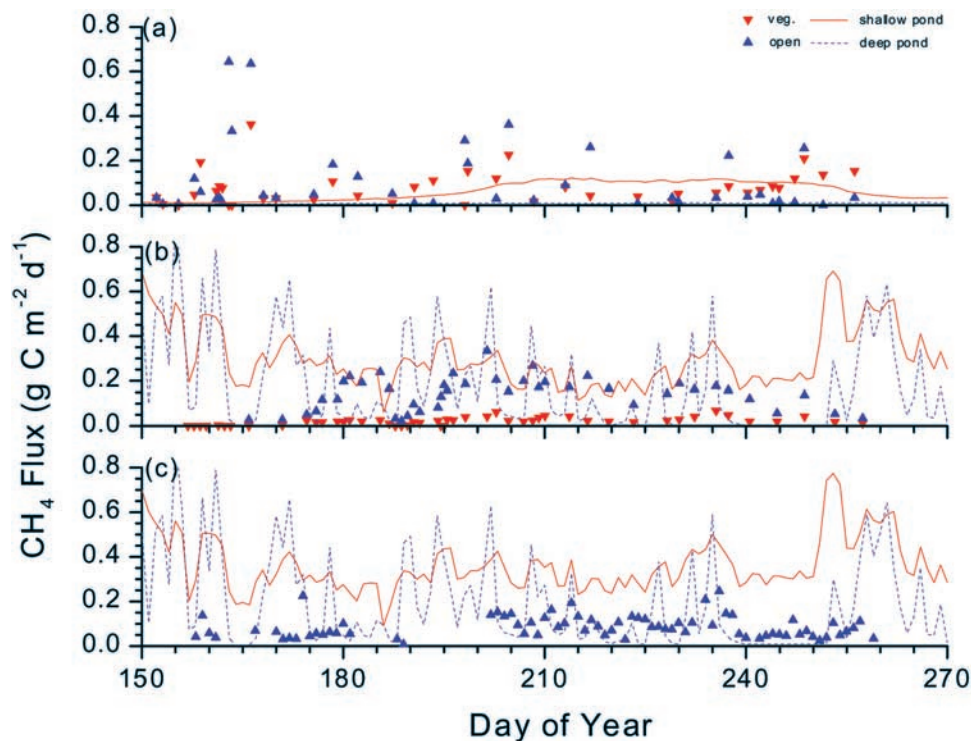


Figure 5. Daily totals of CH_4 effluxes (a) measured with static chambers (symbols) and modeled as soil plus plant diffusion (lines), (b) measured with inverted funnels (symbols) and modeled as bubbling (lines), and (c) measured at the flux tower (symbols) and modeled as diffusion plus bubbling (lines) during 1994. Measured effluxes are from *Dove et al.* [1999].

productivity (equation (1)). Annual net primary productivities (NPP) in the simulated landscape were 388, 621, 286, and 69 g C m^{-2} at the upper slope (sedge plus moss), lower slope (sedge plus moss), shallow pond (sedge), and deep pond (sedge) positions. *Trumbore et al.* [1999] calculated annual NPP of 300–430 g C m^{-2} in nearby poor, intermediate, and rich fens, and 160 g C m^{-2} in a nearby bog collapse.

5.4. Annual CH_4 Effluxes Under Current Climate and Climate Change

[36] Rising C_a , temperature and precipitation projected under the IS92a emissions scenario caused CH_4 effluxes modeled from the beaver pond to rise by $\sim 20\%$ from current rates after 100 years while those from the slope positions changed little (Table 4). In the slope positions, NPP was raised by more rapid CO_2 fixation with higher C_a and air temperatures, and by more rapid N fixation and uptake with higher soil temperatures and longer ice-free seasons [e.g., *Grant and Nalder*, 2000; *Grant et al.*, 2001a]. In the pond positions, however, NPP in the model was constrained by P uptake, and so NPP rose less with rising C_a and temperature. Increased NPP caused more rapid litterfall and heterotrophic respiration and hence greater O_2 demand, while higher soil temperatures reduced O_2 solubility (f_{O_2} in equations (28), (33), (35), (40), and (41)) and hence rates of O_2 dissolution (equations (28) and (35)). Increased demand and reduced solubility caused lower aqueous O_2 concentrations and

thereby greater demand for reduced C as an alternative electron acceptor. In anaerobic soil this demand drove more rapid fermentation (equation (1)) and hence methanogenesis (equations (7) and (12)). These predicted changes in CH_4

Table 3. Seasonal (May–September) Emissions of CH_4 Measured and Modeled From the Beaver Pond Site

Measured		Modeled	
Site	Emissions, g C m^{-2}	Site	Emissions, g C m^{-2}
Moss ^a	0.2	Upper slope ^b	0.35
Mire ^a	94	Lower slope	5.1
Pond ^a	14		
Vegetated pond		Shallow pond	
Diffusive ^c	8.5	Diffusive	7.8
Bubbling ^d	2.2	Bubbling	37.8
Total	10.7	Total	45.6
Open pond		Deep pond	
Diffusive ^d	10.8	Diffusive	0.8
Bubbling ^d	11.8	Bubbling	24.0
Total	22.6	Total	24.8
Pond ^e	8.4		

^a Static chamber measurements from 19 May to 13 September 1994 by *Moosavi and Crill* [1997].

^b Model results are from 20 May to 17 September 1994.

^c Static chamber measurements from 20 May to 15 September 1994 by *Dove et al.* [1999].

^d Inverted funnel measurements from 20 May to 15 September 1994 by *Dove et al.* [1999].

^e Eddy flux measurements from 22 May to 19 September 1994 by *Roulet et al.* [1997].

Table 4. Annual CH₄ Emissions Modeled Under Current Climate and After 100 Years of IS92a-Driven Climate Change (See Table 2)

Landscape Position	Current, g C m ⁻² yr ⁻¹	IS92a, g C m ⁻² yr ⁻¹
Upper slope	1.2	2.8
Lower slope	8.1	7.0
Shallow pond	76.1	94.0
Deep pond	42.9	51.0

emissions were based on the assumption that the pond surface would maintain its current elevation under changing surface hydrology.

6. Discussion

[37] A robust predictive capability for CH₄ emissions from an ecosystem model would help to overcome some limitations of existing techniques in estimating temporally and spatially aggregated emissions. For example brief, rapid effluxes during degassing events caused by soil warming (Figure 4) or drying after rainfall (Figure 3) could either be missed or selectively sampled by periodic chamber measurements, causing under- or over-estimations of annual emissions [Moore *et al.*, 1990]. Furthermore, alteration of surface boundary conditions by static chambers could cause emissions to be underestimated by 20% [Moore and Knowles, 1990; Moore and Roulet, 1995]. These problems can in principle be avoided by continuous, non-intrusive measurements of CH₄ effluxes at flux towers. However, the attribution of spatially aggregated effluxes measured at towers to diverse sources within the tower fetch is problematic, especially under changing wind speeds and directions.

[38] Efforts to test the predictive capability of the model were complicated by the large temporal and spatial variability in the modeled and measured CH₄ effluxes (Figures 3, 4, and 5). The main constraint to model testing was the difficulty in describing spatial variation of site conditions to the model at the small spatial scale at which this variation can affect CH₄ fluxes (<2 m according to Whalen and Reeburgh [1988]). Given the coarse spatial resolution of the simulated landscape (Figure 1), the model was able to simulate the spatial and temporal range of effluxes measured at different sites in the field transect (Figure 3), from the very low values consistently measured at the upland moss site versus those modeled at the upper slope position (<0.05 μmol m⁻² s⁻¹), to the high values periodically measured at the mire site and modeled at the pond positions (>0.5 μmol m⁻² s⁻¹). Daily aggregations of these effluxes modeled at the pond positions encompassed the range of those measured with surface chambers and at the flux tower (0.0–0.3 g m⁻² d⁻¹ in Figure 5), although effluxes from bubbling events in the model were larger than those measured.

[39] The temporal and spatial variation of CH₄ effluxes in the model was achieved from temporal and spatial variation in soil temperature (Figure 3) and water table depth (Figure 1) without any changes in model parameters from those used in earlier studies of methanogenesis and

methanotrophy under laboratory conditions (Appendix A, below, from Grant [1998, 1999]). These parameters were entirely derived from basic microbiological research conducted independently of the model at spatial and temporal scales smaller than those of model testing. This parameterization indicates that the model is likely to provide a robust predictive capability for CH₄ emissions under diverse site conditions. However, better constrained tests of the model under well-described site conditions still needs to be conducted if a more quantitative agreement between measured and modeled effluxes is to be achieved. Further constraint in model testing will require greater temporal resolution in efflux measurements, perhaps through the use of automated surface chambers, in order to monitor individual emission events.

[40] Seasonal totals of CH₄ emissions modeled at the lower slope and pond positions (Table 3) were within ranges of values published for wetlands and ponds [e.g., Moore and Roulet, 1995]. However, CH₄ emissions simulated before late May and after late September caused annual totals in the model (Table 4) to be larger than seasonal totals (Table 3). Emissions simulated during autumn and winter (1 October to 30 April) contributed ~25% to annual totals at the lower slope and shallow pond positions, but only ~5% to that at the deep pond position. Winter emissions from seasonally frozen wetlands have been shown to contribute 4–21% of annual CH₄ totals in peatlands [e.g., Dise, 1992; Mast *et al.*, 1998; Melloh and Crill, 1996]. Brief but rapid emissions simulated during spring thaw in mid-May contributed 20 and 30% to annual totals at the shallow and deep pond positions, respectively. These emissions in the model were driven by the volatilization (equation (28)), transfer (equations (29) and (31)), and release (equations (33) and (34)) of CH₄ that had accumulated under anoxic conditions below ice during the previous winter. Such accumulation has been found in a temperate peatland by Melloh and Crill [1996], and in the beaver pond of this study by Kuhlbusch and Zepp [1999], who estimated winter accumulations to be 6% of summer emissions. Rapid emissions of CH₄ have been frequently observed during spring thaw in northern wetlands [Moore and Knowles, 1990; Moore *et al.*, 1990; Whalen and Reeburgh, 1988; Windsor *et al.*, 1992]. Model testing must therefore be extended to winter and spring periods if confidence in their estimates of annual CH₄ emissions is to be improved.

[41] Model projections indicated that total heterotrophic respiration would rise commensurately with NPP during 100 years of IS92a-driven climate change so that net ecosystem productivity (NEP = NPP - heterotrophic respiration) would not change much from current values. However, CH₄ was projected to remain a stable (deep pond) or gradually rising (shallow pond) fraction of total C emissions from heterotrophic respiration because warming water and sediments caused increased O₂ demand and reduced O₂ solubility. Thus CH₄ emissions were projected to rise by about 20% in boreal ponds after 100 years of IS92a-driven climate change, especially in shallower pond margins which were areas of rapid efflux (Table 4). Given the greater

radiative activity of CH₄ versus CO₂ in the atmosphere, this rise may be the most important impact of climate change on boreal ponds with respect to atmospheric quality. Landscape-level projections of climate change impacts on CH₄ emissions will therefore depend upon the comparative areas of the slope versus pond positions. These areas, especially pond margins that correspond to the shallow pond position in the model, would need to be measured in any attempt to arrive at regional estimates of CH₄ emissions under current versus hypothesized climates.

Appendix A: Equations

A1. Anaerobic Fermenters and H₂ Producing Acetogens

$$R_{i,f} = \{R'_f M_{i,f,a} [P_{i,c}] / (K_f (1 + [O_2]/K_i) [P_{i,c}])\} f_t \quad (1)$$

$$P_{i,c} \rightarrow 0.67 A_{i,c} + 0.33 CO_2 - C + 0.11 H_2 \quad (2)$$

$$U_{i,f,c} = R_{m,i,f} + (R_{i,f} - R_{m,i,f})(1.0 + Y_f) \quad [R_{i,f} > R_{m,i,f}] \quad (3a)$$

$$U_{i,f,c} = R_{i,f} \quad [R_{i,f} < R_{m,i,f}] \quad (3b)$$

$$Y_f = -\Delta G'_f / E_M \quad (4)$$

$$\Delta G'_f = \Delta G'_f + \left\{ RT \ln \left(\frac{[H_2]}{[H'_2]} \right)^4 \right\} \quad (5)$$

$$\delta M_{i,f,j,c} / \delta t = F_j U_{i,f,c} - F_j R_{i,f} - D_{i,f,j,c} \quad [R_{i,f} > R_{m,i,f}] \quad (6a)$$

$$\delta M_{i,f,j,c} / \delta t = F_j U_{i,f,c} - R_{m,i,f,j} - D_{i,f,j,c} \quad [R_{i,f} < R_{m,i,f}] \quad (6b)$$

A2. Acetotrophic Methanogens

$$R_{i,m} = \{R'_m M_{i,m,a} [A_{i,c}] / (K_m + [A_{i,c}])\} f_t \quad (7)$$

$$A_{i,c} \rightarrow 0.50 CH_4 - C + 0.50 CO_2 - C \quad (8)$$

$$U_{i,m,c} = R_{m,i,m} + (R_{i,m} - R_{m,i,m})(1.0 + Y_m) \quad [R_{i,m} > R_{m,i,m}] \quad (9a)$$

$$U_{i,m,c} = R_{i,m} \quad [R_{i,m} < R_{m,i,m}] \quad (9b)$$

$$Y_m = -\Delta G'_m / E_M \quad (10)$$

$$\delta M_{i,m,j,c} / \delta t = F_j U_{i,m,c} - F_j R_{i,m} - D_{i,m,j,c} \quad [R_{i,m} > R_{m,i,m}] \quad (11a)$$

$$\delta M_{i,m,j,c} / \delta t = F_j U_{i,m,c} - R_{m,i,m,j} - D_{i,m,j,c} \quad [R_{i,m} < R_{m,i,m}] \quad (11b)$$

A3. Hydrogenotrophic Methanogens

$$R_h = \{R'_h M_{h,a} [H_2] / (K_h + [H_2]) [CO_2] / (K_c [CO_2])\} f_t \quad (12)$$

$$CO_2 - C + 0.67 H_2 \rightarrow CH_4 - C + 3 H_2O \quad (13)$$

$$U_{h,c} = R_{m,h} + (R_h - R_{m,h})(1.0 + Y_h) \quad [R_h > R_{m,h}] \quad (14a)$$

$$U_{h,c} = R_h \quad [R_h < R_{m,h}] \quad (14b)$$

$$Y_h = -\Delta G'_h / E_C \quad (15)$$

$$\Delta G'_h = \Delta G'_h - \left\{ RT \ln \left(\frac{[H_2]}{[H'_2]} \right)^4 \right\} \quad (16)$$

$$\delta M_{h,j,c} / \delta t = F_j U_{h,c} - F_j R_h - D_{h,j,c} \quad [R_h > R_{m,h}] \quad (17a)$$

$$\delta M_{h,j,c} / \delta t = F_j U_{h,c} - R_{m,h,j} - D_{h,j,c} \quad [R_h < R_{m,h}] \quad (17b)$$

A4. Autotrophic Methanotrophs

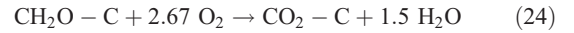
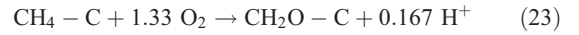
$$X'_t = \{X'_t M_{t,a} [CH_4] / (K_t + [CH_4])\} f_t \quad (18)$$

$$R'_t = X'_t Y_{tR} \quad (19)$$

$$Y_{tR} = -\Delta G'_t / E_G \quad (20)$$

$$X_t = X'_t f_{o_2 t} \quad (21a)$$

$$R_t = R'_t f_{o_2 t} \quad (21b)$$



$$U_{t,c} = R_{m,t} + (R_t - R_{m,t})(1.0 + Y_{tG}) \quad [R_t > R_{m,t}] \quad (25a)$$

$$U_{t,c} = R_t \quad [R_t < R_{m,t}] \quad (25b)$$

$$Y_{tG} = -\Delta G'_t / E_M \quad (26)$$

$$\delta M_{t,j,c} / \delta t = F_j U_{t,c} - F_j R_t - D_{t,j,c} \quad [R_t > R_{m,t}] \quad (27a)$$

$$\delta M_{t,j,c} / \delta t = F_j U_{t,c} - R_{m,t,j} - D_{t,j,c} \quad [R_t < R_{m,t}] \quad (27b)$$

A5. Transport of Reactants and Products

A5.1. Aqueous and Gaseous Diffusion in Soil

$$T_{\gamma s} = a_{gs} D_{t\gamma} (S'_{\gamma} f_{t\gamma} [\gamma_{gs}] - [\gamma_{ss}]) \quad (28)$$

$$Q_{ss\gamma} = Q_w [\gamma_{ss}] + D_{ss\gamma} \Delta [\gamma_{ss}] / \Delta z \quad (29)$$

$$D_{ss\gamma} = \lambda |Q_w| + D'_{s\gamma} f_{t\gamma} \tau_s \theta_s^{vis} \quad (30)$$

$$Q_{sg\gamma} = -Q_w [\gamma_g] + D_{gs\gamma} \Delta [\gamma_{gs}] / \Delta z \quad (31)$$

$$Q_{sg\gamma} = D'_{s\gamma} f_{t\gamma} \theta_s^{vis} / \theta_p^2 \quad (32)$$

$$Q'_{ss\gamma} = g_a \{ [\gamma_a] - \{ [\gamma_{ss}] D_{ss\gamma} / (0.5 \Delta z') + g_a [\gamma_a] \} / \{ D_{ss\gamma} S'_{t\gamma} / (0.5 \Delta z') + g_a \} \} \quad (33)$$

$$Q'_{gs\gamma} = g_a \{ [\gamma_a] - \{ [\gamma_{gs}] D_{gs\gamma} / (0.5 \Delta z') + g_a [\gamma_a] \} / \{ D_{gs\gamma} / (0.5 \Delta z') + g_a \} \} \quad (34)$$

A5.2. Aqueous and Gaseous Diffusion in Plants

$$T_{\gamma r} = a_{gr} D_{t\gamma} (S'_{\gamma} f_{t\gamma} [\gamma_{gr}] - [\gamma_{sr}]) \quad (35)$$

$$Q_{sr\gamma} = U_w [\gamma_{ss}] + 2\pi L_r D_{sr\gamma} \Delta ([\gamma_{ss}] - [\gamma_{sr}]) / \ln(d_r/r_r) \quad (36)$$

$$D_{sr\gamma} = \lambda |U_w| + D'_{s\gamma} f_{t\gamma} \tau_s \theta_s^{vis} \quad (37)$$

$$Q_{gr\gamma} = D_{gr\gamma} ([\gamma_a] - [\gamma_{gr}]) / \Delta z_r \quad (38)$$

$$D_{gr\gamma} = D'_{g\gamma} f_{t\gamma} \theta_{gr}^{vis} A_r \quad (39)$$

A5.3. Bubbling

$$Q_{b\gamma} = \min \left\{ 0, p / (RT) - \sum [\gamma_{gs}]' \right\} \left([\gamma_{gs}]' / \sum [\gamma_{gs}]' \right) \cdot S'_{\gamma} f_{t\gamma} M_{\gamma} V_w \quad (40)$$

$$\sum_{\gamma} [\gamma_{gs}]' = \sum_{\gamma} \left\{ [\gamma_{ss}]' / (S'_{\gamma} f_{t\gamma} M_{\gamma} V_w) \right\} \quad (41)$$

Appendix B: Glossary

A	acetate (g C m ⁻²) [2] ¹¹	$\Delta G'_f$	ΔG_f when [H ₂] = [H ₂ '] (kJ g P _{i, c} ⁻¹) [5]
[A]	aqueous concentration of acetate (g C m ⁻³) [7]	ΔG_h	free energy change of hydrogenotrophic methanogenesis (kJ g CO ₂ -C ⁻¹) [15, 16]
A _r	total cross-sectional area of root axes (m ² m ⁻²) [39]	$\Delta G'_h$	free energy change of hydrogenotrophic methanogenesis when [H ₂] = [H ₂ '] (kJ g CO ₂ -C ⁻¹) [16]
<i>a</i>	descriptor for <i>j</i> = active component of M _{<i>i</i>}	$\Delta G'_m$	free energy change of acetotrophic methanogenesis (kJ g A _{<i>i, c</i>} ⁻¹) [10]
a _{gr}	air-water interfacial area in root (m ² m ⁻²) [35]	$\Delta G'_t$	free energy change of CH ₄ oxidation by methanotrophs (kJ g CH ₄ -C ⁻¹) [20]
a _{gs}	air-water interfacial area in soil (m ² m ⁻²) [28]	g _a	boundary layer conductance between the atmosphere and the soil surface (h m ⁻¹) [33, 34]
[CH ₄]	aqueous concentration of CH ₄ (g C m ⁻³) [18]	[γ _a]	concentration of gas γ in the atmosphere (g m ⁻³) [33, 34, 38]
[CO ₂]	aqueous concentration of CO ₂ (g C m ⁻³) [12]	[γ _a ']	concentration of gas γ in the atmosphere (mol m ⁻³) [40]
D _{<i>h, j, c</i>}	decomposition of hydrogenotrophic methanogens (g C m ⁻² h ⁻¹) [17a, 17b]	[γ _{gr}]	concentration of gas γ in the gaseous phase of the root (g m ⁻³) [35, 38]
D _{<i>i, f, j, c</i>}	decomposition of fermenters and acetogens (g C m ⁻² h ⁻¹) [6a, 6b]	[γ _{gs}]	concentration of gas γ in the gaseous phase of the soil (g m ⁻³) [28, 31, 34]
D _{<i>i, m, j, c</i>}	decomposition of acetotrophic methanogens (g C m ⁻² h ⁻¹) [11a, 11b]	[γ _{gs} ']	concentration of gas γ in the gaseous phase of the soil in equilibrium with [γ _{ss}] (mol m ⁻³) [40, 41]
D _{<i>t, j, c</i>}	decomposition of autotrophic methanotrophs (g C m ⁻² h ⁻¹) [27a, 27b]	[γ _{sr}]	concentration of gas γ in the aqueous phase of the root (g m ⁻³) [35, 36]
D _{grγ}	gaseous diffusivity of gas γ during vertical transport in root (m ² h ⁻¹) [38, 39]	[γ _{ss}]	concentration of gas γ in the aqueous phase of the soil (g m ⁻³) [28, 29, 33, 37, 41]
D _{gsγ}	gaseous diffusivity of gas γ during vertical transport in soil (m ² h ⁻¹) [31, 32, 34]	[H ₂]	aqueous concentration of H ₂ (g m ⁻³) [5, 12, 16]
D' _{gγ}	gaseous diffusivity of gas γ in air at 30°C (m ² h ⁻¹) [32, 39]	[H ₂ ']	aqueous concentration of H ₂ when $\Delta G_h = \Delta G'_h$ and $\Delta G_f = \Delta G'_f$ (g H m ⁻³) [5, 16]
D _{srγ}	aqueous dispersivity-diffusivity of gas γ during root uptake in soil (m ² h ⁻¹) [36, 37]	<i>h</i>	descriptor for hydrogenotrophic methanogens in each M _{<i>i</i>}
D _{ssγ}	aqueous dispersivity-diffusivity of gas γ during vertical transport in soil (m ² h ⁻¹) [29, 30, 33]	<i>i</i>	descriptor for organic matter-microbe complex (<i>i</i> = plant residue, manure, particulate OM, or humus)
D' _{svγ}	aqueous diffusivity of gas γ in water at 30°C (m ² h ⁻¹) [30, 37]	<i>j</i>	descriptor for structural or kinetic components for each functional type within each M _{<i>i</i>} (e.g., <i>a</i> = active)
D _{tvγ}	volatilization-dissolution transfer coefficient (m h ⁻¹) [28, 35]	K _{<i>c</i>}	M-M constant for uptake of CO ₂ by hydrogenotrophic methanogens (g C m ⁻³) [12]
d _r	half-distance between adjacent roots (m) [36]	K _{<i>f</i>}	M-M constant for uptake of P _{<i>i, c</i>} by fermenters and acetogens (g C m ⁻³) [1]
E _C	energy required to construct new M from CO ₂ (kJ g C ⁻¹) [15]	K _{<i>h</i>}	M-M constant for uptake of H ₂ by hydrogenotrophic methanogens (g H m ⁻³) [12]
E _G	energy required to transform CH ₄ into organic C (kJ g C ⁻¹) [20]	K _{<i>m</i>}	M-M constant for uptake of A _{<i>i, c</i>} by acetotrophic methanogens (g C m ⁻³) [7]
E _M	energy required to construct new M from organic C (kJ g C ⁻¹) [4, 10, 26]	K _{<i>t</i>}	M-M constant for uptake of CH ₄ by methanotrophs (g C m ⁻³) [18]
F _{<i>j</i>}	partitioning coefficient for <i>j</i> in M _{<i>i, n, j</i>} [6a, 6b, 11a, 11b, 17a, 17b, 27a, 27b]	<i>k</i>	descriptor for elemental fraction within each <i>j</i> (<i>j</i> = <i>c, n</i> , or <i>p</i>)
<i>f</i>	descriptor for fermenters and acetogens in each M _{<i>i</i>}	L _r	root length (m m ⁻²) [36]
<i>f</i> _{o₂<i>t</i>}	ratio of O ₂ uptake to O ₂ requirement for CH ₄ oxidation [21a, 21b]	λ	hydrodynamic dispersion coefficient (m) [30, 37]
<i>f</i> _t	temperature function for growth-related processes (dimensionless) [1, 7, 12]	M	microbial communities (g C m ⁻²)
<i>f</i> _{ig}	temperature function for gaseous diffusivity (dimensionless) [32, 39]	M _{<i>h</i>}	hydrogenotrophic methanogen community (g C m ⁻²) [12, 17a, 17b]
<i>f</i> _{ta}	temperature function for aqueous diffusivity (dimensionless) [30, 37]	M _{<i>i, f</i>}	fermenter and acetogenic community (g C m ⁻²) [1, 6a, 6b]
<i>f</i> _{tsγ}	temperature function for solubility of gas γ (dimensionless) [28, 33, 35, 40, 41]	M _{<i>i, m</i>}	acetotrophic methanogen community (g C m ⁻²) [7, 11a, 11b]
$\Delta G'_c$	free energy change of C oxidation-O ₂ reduction (kJ g C ⁻¹) [26]		
ΔG_f	free energy change of fermentation plus acetogenesis (kJ g P _{<i>i, c</i>} ⁻¹) [4, 5]		

¹ Numbers in brackets refer to equations above in which variable is used.

M_t	autotrophic methanotrophic community (g C m ⁻²) [18, 27a, 27b]	R'_t	CH ₄ oxidation by methanotrophs for respiration at saturating O ₂ (g C m ⁻² h ⁻¹) [19, 21b]
M_γ	molecular mass of gas γ (g mol ⁻¹) [40, 41]	r_r	root radius (m) [36]
m	descriptor for acetotrophic methanogens in each M_i	S'_γ	Ostwald solubility coefficient of gas γ at 30 °C (m ³ air m ³ water) [28, 33, 35, 40, 41]
P	soluble organic matter (g C m ⁻²)	T	soil temperature (K) [5, 16, 40]
[P]	aqueous concentration of soluble organic matter (g C m ⁻³) [1]	t	descriptor for autotrophic methanotrophs
p	atmospheric pressure (kPa) [40]	$T_{\gamma r}$	exchange of gas γ between gaseous and aqueous phases in the root (g m ⁻² h ⁻¹) [35]
$Q_{b\gamma}$	bubble transport of gas γ in the aqueous phase of the soil (g m ⁻² h ⁻¹) [40]	$T_{\gamma s}$	exchange of gas γ between gaseous and aqueous phases in the soil (g m ⁻² h ⁻¹) [28]
$Q_{gr\gamma}$	vertical transport of gas γ in the gaseous phase of the root (g m ⁻² h ⁻¹) [38]	τ_g	tortuosity coefficient for gaseous diffusion [32, 33]
$Q_{gs\gamma}$	vertical transport of gas γ in the gaseous phase of the soil (g m ⁻² h ⁻¹) [31]	τ_s	tortuosity coefficient for aqueous diffusion [30, 37]
$Q'_{gs\gamma}$	vertical transport of gas γ between the atmosphere and the gaseous phase of the soil surface (g m ⁻² h ⁻¹) [34]	$U_{h,c}$	rate of CO ₂ uptake by M_h (g C m ⁻² h ⁻¹) [14a, 14b, 17a, 17b, 18]
$Q_{sr\gamma}$	root uptake of gas γ in the aqueous phase of the soil (g m ⁻² h ⁻¹) [36]	$U_{i,f,k}$	rate of $P_{i,k}$ uptake by $M_{i,f}$ (g C m ⁻² h ⁻¹) [3a, 3b, 6a, 6b]
$Q_{ss\gamma}$	vertical transport of gas γ in the aqueous phase of the soil (g m ⁻² h ⁻¹) [29]	$U_{i,m,c}$	rate of $A_{i,c}$ uptake by $M_{i,m}$ (g C m ⁻² h ⁻¹) [9a, 9b, 11a, 11b]
$Q'_{ss\gamma}$	vertical transport of gas γ between the atmosphere and the aqueous phase of the soil surface (g m ⁻² h ⁻¹) [33]	$U_{t,c}$	rate of CH ₄ uptake by M_t (g C m ⁻² h ⁻¹) [25a, 25b, 27a, 27b]
Q_w	vertical transport of water (m ³ m ⁻² h ⁻¹) [29, 30, 31]	U_w	root uptake of water (m ³ m ⁻² h ⁻¹) [36, 37]
θ_{gr}	root air-filled porosity (m ³ m ⁻³) [39]	V_w	volume of water in soil (m ³ m ⁻²) [40]
θ_{gs}	soil air-filled porosity (m ³ m ⁻³) [32]	v_{gr}	sensitivity of τ_g to θ_{gr} [39]
θ_p	soil total porosity (m ³ m ⁻³) [33]	v_{gs}	sensitivity of τ_g to θ_{gs} [32]
θ_s	soil water content (m ³ m ⁻³) [30, 37]	v_s	sensitivity of τ_s to θ_s [30, 37]
R	gas constant (kJ mol ⁻¹ K ⁻¹) [5, 16, 40]	X_t	CH ₄ oxidation by methanotrophs (g C m ⁻² h ⁻¹) [21a, 22]
R'_f	specific respiration by fermenters and acetogens at saturating [P _{i,c}], 30°C and high water potential (g C g M _{i,f,a} ⁻¹ h ⁻¹) [1]	X'_t	CH ₄ oxidation by methanotrophs at saturating O ₂ (g C m ⁻² h ⁻¹) [1, 2, 4]
R_h	CO ₂ reduction by hydrogenotrophic methanogens (g C m ⁻² h ⁻¹) [12, 13, 14a, 14b, 17a, 17b, 18]	X'_t	specific CH ₄ oxidation by methanotrophs at saturating O ₂ , 30 °C and high water potential (g C g ⁻¹ h ⁻¹) [18]
R'_h	specific CO ₂ reduction by hydrogenotrophic methanogens at saturating [H ₂] and [CO ₂], and at 30°C and high water potential (g C g M _{h,a} ⁻¹ h ⁻¹) [12]	Y_f	biomass yield from fermentation and acetogenic reactions (g M _{i,f} g P _{i,c} ⁻¹) [3a, 3b, 4]
$R_{i,f}$	respiration of hydrolysis products by fermenters and acetogens (g C m ⁻² h ⁻¹) [1, 2, 3a, 3b, 6a, 6b]	Y_h	biomass yield from hydrogenotrophic methanogenic reaction (g M _h g CO ₂ -C ⁻¹) [14a, 14b, 15, 18]
$R_{i,m}$	respiration of acetate by acetotrophic methanogens (g C m ⁻² h ⁻¹) [7, 8, 9a, 9b, 11a, 11b]	Y_m	biomass yield from acetotrophic methanogenic reaction (g M _{i,m} g A _{i,c} ⁻¹) [9a, 9b, 10]
R'_m	specific respiration by acetotrophic methanogens at saturating [A _{i,c}], 30 °C and high water potential (g C g M _{i,m,a} ⁻¹ h ⁻¹) [7]	Y_{t_g}	biomass yield from methanotrophic growth respiration (g M _t -C g CH ₄ -C ⁻¹) [25a, 26]
$R_{mh,j}$	maintenance respiration by hydrogenotrophic methanogens (g C m ⁻² h ⁻¹) [14a, 14b, 17a, 17b]	Y_{r_r}	ratio of CH ₄ respired versus CH ₄ oxidized by methanotrophs (g C g C ⁻¹) [19, 20]
$R_{mi,f,j}$	maintenance respiration by fermenters and acetogens (g C m ⁻² h ⁻¹) [3a, 3b, 6a, 6b]	z	depth to midpoint of soil layer (m) [29, 31]
$R_{mi,m,j}$	maintenance respiration by acetotrophic methanogens (g C m ⁻² h ⁻¹) [9a, 9b, 11a, 11b]	z_r	depth to midpoint of soil layer + average root axis length (m) [38]
$R_{mt,j}$	maintenance respiration by methanotrophs (g C m ⁻² h ⁻¹) [25a, 25b, 27a, 27b]	z'	depth to midpoint of soil surface layer (m) [33, 34]
R_t	CH ₄ oxidation by methanotrophs for respiration (g C m ⁻² h ⁻¹) [21b, 23, 24, 25a, 25b, 27a]		

[42] **Acknowledgments.** Computational facilities were provided by the Multimedia Advanced Computational Initiative (MACI) at the Universities of Alberta and Calgary. This work contributes to the Global Change Terrestrial Ecosystem (GCTE) Core Research Programme, which is part of the International Geosphere-Biosphere Programme (IGBP).

References

Amthor, J. S., et al., Boreal forest CO₂ exchange and evapotranspiration predicted by nine ecosystem process models: Inter-model comparisons

- and relationships to field measurements, *J. Geophys. Res.*, *106*, 33,623–33,648, 2001.
- Anthony, C., *The Biochemistry of Methylophils*, Academic, San Diego, Calif., 1982.
- Aselmann, I., and D. J. Crutzen, A global inventory of wetland distribution and seasonality, net primary productivity, and estimated methane emissions, in *Soils and the Greenhouse Effect*, edited by A. F. Bouwman, pp. 441–449, John Wiley, New York, 1990.
- Bartlett, K. B., and R. C. Harriss, Review and assessment of methane emissions from wetlands, *Chemosphere*, *26*, 261–320, 1993.
- Billen, G., Modelling the process of organic matter degradation and nutrient cycling in sedimentary systems, in *Sediment Microbiology*, edited by D. B. Nedwell and C. M. Brown, pp. 15–52, Academic, San Diego, Calif., 1982.
- BOREAS TF-03, NSA-OBS Tower flux, Meteorological, and Soil Temperature Data, <http://www-eosdis.ornl.gov/>, ORNL Distrib. Active Arch. Cent., Oak Ridge Natl. Lab., Oak Ridge, Tenn., 1998.
- BOREAS TGB-01, Soil CH₄ and CO₂ Profile Data from NSA Tower Sites, <http://www-eosdis.ornl.gov/>, ORNL Distrib. Active Arch. Cent., Oak Ridge Natl. Lab., Oak Ridge, Tenn., 1998.
- Brock, T. D., and M. T. Madigan, *Biology of Microorganisms*, 6th ed., Prentice-Hall, Old Tappan, N.J., 1991.
- Cao, M., J. B. Dent, and O. W. Heal, Modeling methane emissions from rice paddies, *Global Biogeochem. Cycles*, *9*, 183–195, 1995.
- Cicerone, R. J., and R. Oremland, Biogeochemical aspects of atmospheric methane, *Global Biogeochem. Cycles*, *4*, 299–327, 1988.
- Conrad, R., Capacity of aerobic microorganisms to utilize and grow on atmospheric trace gases (H₂, CO, CH₄), in *Current Perspectives in Microbial Ecology*, edited by M. J. Klug and C. A. Reddy, pp. 461–467, Am. Soc. of Microbiol., Washington, D. C., 1984.
- Dalva, M., T. R. Moore, P. Arp, and T. A. Clair, Methane and soil and plant community respiration from wetlands, Kejimikujik National Park, Nova Scotia: Measurements, predictions and climatic change, *J. Geophys. Res.*, *106*, 2955–2962, 2001.
- Dise, N. B., Winter fluxes from Minnesota peatlands, *Biogeochemistry*, *16*, 71–83, 1992.
- Dove, A., N. Roulet, P. Crill, J. Chanton, and R. Bourbonniere, Methane dynamics of a northern boreal beaver pond, *Ecoscience*, *6*, 577–586, 1999.
- Dunfield, P., R. Knowles, R. Dumont, and T. R. Moore, Methane production and consumption in temperate and subarctic peat soils: Response to temperature and pH, *Soil Biol. Biochem.*, *25*, 321–326, 1993.
- Fechner, E., and H. F. Hemond, Methane transport and oxidation in the unsaturated zone of a Sphagnum peatland, *Global Biogeochem. Cycles*, *6*, 33–44, 1992.
- Friborg, T., T. R. Christensen, B. U. Hansen, C. Nordstroem, and H. Soegaard, Trace gas exchange in a high arctic valley, 2, Landscape CH₄ fluxes measured and modeled using eddy correlation data, *Global Biogeochem. Cycles*, *14*, 715–723, 2000.
- Frolking, S., and P. Crill, Climate controls on temporal variability of methane flux from a poor fen in southeastern New Hampshire: Measurement and modeling, *Global Biogeochem. Cycles*, *8*, 299–327, 1994.
- Fung, I. Y., J. J. Lerner, E. Matthews, M. Prather, L. P. Steele, and P. J. Fraser, Three-dimensional model synthesis of global methane cycle, *J. Geophys. Res.*, *96*, 13,033–13,065, 1991.
- Grant, R. F., Simulation model of soil compaction and root growth, I, Model development, *Plant Soil*, *150*, 1–14, 1993.
- Grant, R. F., Simulation of ecological controls on nitrification, *Soil Biol. Biochem.*, *26*, 305–315, 1994.
- Grant, R. F., Mathematical modelling of nitrous oxide evolution during nitrification, *Soil Biol. Biochem.*, *27*, 1117–1125, 1995.
- Grant, R. F., Simulation of methanogenesis in the mathematical model Ecosys, *Soil Biol. Biochem.*, *30*, 883–896, 1998.
- Grant, R. F., Simulation of methanotrophy in the mathematical model Ecosys, *Soil Biol. Biochem.*, *31*, 287–297, 1999.
- Grant, R. F., A review of the Canadian ecosystem model Ecosys, in *Modeling Carbon and Nitrogen Dynamics for Soil Management*, edited by M. Shaffer, pp. 175–264, CRC, Boca Raton, Fla., 2001.
- Grant, R. F., and I. A. Nalder, Climate change effects on net carbon exchange of a boreal aspen-hazelnut forest: Estimates from the ecosystem model Ecosys, *Global Change Biol.*, *6*, 183–200, 2000.
- Grant, R. F., and E. Patey, Mathematical modeling of nitrous oxide emissions from an agricultural field during spring thaw, *Global Biogeochem. Cycles*, *13*, 679–694, 1999.
- Grant, R. F., and P. Rochette, Soil microbial respiration at different temperatures and water potentials: Theory and mathematical modeling, *Soil Sci. Soc. Am. J.*, *58*, 1681–1690, 1994.
- Grant, R. F., N. G. Juma, and W. B. McGill, Simulation of carbon and nitrogen transformations in soils, I, Mineralization, *Soil Biol. Biochem.*, *25*, 1317–1329, 1993a.
- Grant, R. F., N. G. Juma, and W. B. McGill, Simulation of carbon and nitrogen transformations in soils, II, Microbial biomass and metabolic products, *Soil Biol. Biochem.*, *25*, 1331–1338, 1993b.
- Grant, R. F., M. Nyborg, and J. Laidlaw, Evolution of nitrous oxide from soil, I, Model development, *Soil Sci.*, *156*, 259–265, 1993c.
- Grant, R. F., M. Nyborg, and J. Laidlaw, Evolution of nitrous oxide from soil, II, Experimental results and model testing, *Soil Sci.*, *156*, 266–277, 1993d.
- Grant, R. F., R. C. Izaurralde, and D. S. Chanasyk, Soil temperature under different surface managements: Testing a simulation model, *Agric. For. Meteorol.*, *73*, 89–113, 1995.
- Grant, R. F., M. L. Goulden, S. C. Wofsy, and J. A. Berry, Carbon and energy exchange by a black spruce-moss ecosystem under changing climate: Testing the mathematical model Ecosys with data from the BOREAS experiment, *J. Geophys. Res.*, *106*, 33,605–33,621, 2001a.
- Grant, R. F., N. G. Juma, J. A. Robertson, and W. B. McGill, Long term changes in soil C under different fertilizer, manure and rotation: Testing the mathematical model Ecosys with data from the Breton Plots, *Soil Sci. Soc. Am. J.*, *65*, 205–214, 2001b.
- Imboden, D. M., and R. P. Schwarzenbach, Spatial and temporal distribution of chemical substances in lakes: Modeling concepts, in *Chemical Processes in Lakes*, edited by W. Stumm, pp. 1–30, John Wiley, New York, 1985.
- Kattenberg, A., F. Giorgi, H. Grassl, G. A. Meehl, J. F. B. Mitchell, R. J. Stouffer, T. Tokioka, A. J. Weaver, and T. M. L. Wigley, Climate models: Projection of future climate, in *Climate Change 1995: The Science of Climate Change*, edited by J. T. Houghton et al., pp. 285–357, Cambridge Univ. Press, New York, 1996.
- Kuhlbusch, T. A. J., and R. G. Zepp, Carbon trace gases in lake and beaver pond ice near Thompson, Manitoba, Canada, *J. Geophys. Res.*, *104*, 27,693–27,698, 1999.
- Lawrence, A. L., Anaerobic biological treatment processes, *Adv. Chem. Ser.*, *105*, 163–189, 1971.
- Luxmoore, R. J., L. H. Stolzy, and J. Letey, Oxygen diffusion in the soil-plant system, I, A model, *Agron. J.*, *62*, 317–322, 1970.
- Martikainen, P. J., N. Hannu, P. Crill, and J. Silvila, The effect of changing water table on methane fluxes at two Finnish mire sites, *Suo*, *43*, 237–240, 1993.
- Mast, M. A., K. P. Wickland, R. T. Striegl, and D. W. Clow, Winter fluxes of CO₂ and CH₄ from subalpine soils in Rocky Mountain National Park, Colorado, *Global Biogeochem. Cycles*, *12*, 607–620, 1998.
- McGill, W. B., H. W. Hunt, R. G. Woodmansee, and J. O. Reuss, Phoenix, a model of the dynamics of carbon and nitrogen in grassland soils, *Ecol. Bull.*, *33*, 49–115, 1981.
- Melillo, J. M., I. C. Prentice, G. D. Farquhar, E.-D. Schulzeau, and O. E. Sala, Terrestrial biotic responses to environmental change and feedbacks to climate, in *Climate Change 1995: The Science of Climate Change*, edited by J. T. Houghton et al., pp. 445–481, Cambridge Univ. Press, New York, 1996.
- Melloh, R. A., and P. M. Crill, Winter methane dynamics in a temperate peatland, *Global Biogeochem. Cycles*, *10*, 247–254, 1996.
- Millington, R. J., Gas diffusion in porous media, *Science*, *130*, 100–102, 1959.
- Moore, T. R., and R. Knowles, Methane emissions from fen, bog and swamp peatlands in Quebec, *Biogeochemistry*, *11*, 45–61, 1990.
- Moore, T. R., and N. T. Roulet, Methane emission from Canadian peatlands, in *Soils and Global Change*, edited by R. Lal et al., pp. 153–164, CRC, Boca Raton, Fla., 1995.
- Moore, T., N. Roulet, and R. Knowles, Spatial and temporal variations of methane flux from subarctic/northern boreal fens, *Global Biogeochem. Cycles*, *4*, 29–46, 1990.
- Moosavi, S. C., and P. M. Crill, Controls on CH₄ and CO₂ emissions along two moisture gradients in the Canadian boreal zone, *J. Geophys. Res.*, *102*, 29,261–29,277, 1997.
- Mosey, F. E., Kinetic descriptions of anaerobic digestion, paper presented at Third International Symposium on Anaerobic Digestion, Boston Univ., Cambridge, Mass., 1983.
- Potter, C., J. Bubier, P. Crill, and P. Lafleur, Ecosystem modeling of methane and carbon dioxide fluxes for boreal forest sites, *Can. J. For. Res.*, *31*, 208–223, 2001.
- Robinson, J. A., and J. M. Tiedje, Kinetics of hydrogen consumption by rumen fluid, digester sludge and sediment, *Appl. Environ. Microbiol.*, *44*, 1374–1384, 1982.
- Roulet, N. T., R. Ash, and T. R. Moore, Low boreal wetlands as a source of atmospheric methane, *J. Geophys. Res.*, *97*, 3739–3749, 1992.
- Roulet, N. T., P. M. Crill, N. T. Comer, A. Dove, and R. A. Bourbonniere,

- CO₂ and CH₄ flux between a boreal beaver pond and the atmosphere, *J. Geophys. Res.*, *102*, 29,313–29,319, 1997.
- Schink, B., Energetics of syntrophic cooperation in methanogenic degradation, *Microbiol. Mol. Biol. Rev.*, *61*, 262–280, 1997.
- Segers, R., and P. A. Leffelaar, Modeling methane fluxes in wetlands with gas-transporting plants, 1, Single-root scale, *J. Geophys. Res.*, *106*, 3511–3528, 2001a.
- Segers, R., and P. A. Leffelaar, Modeling methane fluxes in wetlands with gas-transporting plants, 3, Plot scale, *J. Geophys. Res.*, *106*, 3541–3558, 2001b.
- Shea, T. G., W. E. Pretorius, R. D. Cole, and E. A. Pearson, Kinetics of hydrogen assimilation in the methane fermentation, *Water Res.*, *2*, 833–848, 1968.
- Smith, M. R., and R. A. Mah, Growth and methanogenesis by *Methanosarcina* strain 227 on acetate and methanol, *Appl. Environ. Microbiol.*, *36*, 870–879, 1978.
- Smith, M. R., and R. A. Mah, Acetate as sole carbon and energy source for growth of *Methanosarcina* strain 227, *Appl. Environ. Microbiol.*, *39*, 993–999, 1980.
- Trumbore, S. E., J. L. Bubier, J. W. Harden, and P. M. Crill, Carbon cycling in boreal wetlands: A comparison of three approaches, *J. Geophys. Res.*, *104*, 27,673–27,682, 1999.
- Walter, B. P., and M. Heimann, A process-based, climate-sensitive model to derive methane emissions from natural wetlands: Application to five wetland sites, sensitivity to model parameters, and climate, *Global Biogeochem. Cycles*, *14*, 745–765, 2000.
- Whalen, S. C., and W. S. Reece, A CH₄ time series for tundra environments, *Global Biogeochem. Cycles*, *2*, 399–409, 1988.
- Whiting, G. J., and J. P. Chanton, Plant-dependent CH₄ emission in a subarctic Canadian fen, *Global Biogeochem. Cycles*, *6*, 225–231, 1992.
- Wilhelm, E., R. Battino, and R. J. Wilcock, Low-pressure solubility of gases in liquid water, *Chem. Rev.*, *77*, 219–262, 1977.
- Windsor, J., T. R. Moore, and N. T. Roulet, Episodic fluxes of methane from subarctic fens, *Can. J. Soil Sci.*, *72*, 441–452, 1992.
- Wofford, N. G., P. S. Beaty, and M. J. McInerney, Preparation of cell-free extracts and the enzymes involved in fatty acid metabolism in *Syntrophomonas wolfei*, *J. Bacteriol.*, *167*, 189–195, 1986.
- Zehnder, A. J. B., and K. Wuhrmann, Physiology of a *Methanobacterium* strain AZ, *Arch. Microbiol.*, *111*, 199–205, 1977.
- Zehnder, A. J. B., B. A. Huser, T. D. Brock, and K. Wuhrmann, Characterization of an acetate-decarboxylating, non-hydrogen-oxidizing methane bacterium, *Arch. Microbiol.*, *124*, 1–11, 1980.

R. F. Grant, Department of Renewable Resources, University of Alberta, 442 Earth Science Building, Edmonton, Alberta T6G 2E1, Canada. (robert.grant@ualberta.ca)

N. T. Roulet, Department of Geography and Centre for Climate and Global Change Research, McGill University, 805 Sherbrooke Street West, Montreal, Quebec H3A 2K6, Canada. (roulet@felix.geog.mcgill.ca)